Advances in Geo-Energy Research

Vol. 11, No. 3, p. 168-180, 2024

Original article

Pyrolysis behavior and pyrolysate characteristics of Huadian oil shale kerogen catalyzed by nickel-modified montmorillonite

Jingjing Gu[1,2,3], Sunhua Deng[1,2,3]*, Youhong Sun[2,3,4], Wei Guo[1,2,3], Han Chen[1], Boyu Shi[1]

[1]*College of Construction Engineering, Jilin University, Changchun 130026. P. R. China*
[2]*National-Local Joint Engineering Laboratory of In-situ Conversion, Drilling and Exploitation Technology for Oil Shale, Jilin University, Changchun 130026, P. R. China.*
[3]*Key Lab of Ministry of Natural Resources for Drilling and Exploitation Technology in Complex Conditions, Jilin University, Changchun 130026. P. R. China*
[4]*School of Engineering and Technology, China University of Geosciences (Beijing), Beijing 100083, P. R. China*

Keywords:
Oil shale
kerogen
catalytic pyrolysis
modified montmorillonite

Cited as:
Gu, J., Deng, S., Sun, Y., Guo, W., Chen, H., Shi, B. Pyrolysis behavior and pyrolysate characteristics of Huadian oil shale kerogen catalyzed by nickel-modified montmorillonite. Advances in Geo-Energy Research, 2024, 11(3): 168-180.
https://doi.org/10.46690/ager.2024.03.02

Abstract:
Given the abundance of clay minerals in oil shales, the in-situ cracking of oil shale is preferably enhanced by catalysis, such as by modifying reservoir clays with soluble catalytically active materials. In this work, nickel-modified montmorillonite was synthesized via a simple method, and the feasibility of in-situ catalytic cracking of oil shales to facilitate engineering implementation was investigated. Thermogravimetric analysis was performed to assess the impact of the catalyst on the pyrolysis behavior of kerogen. The results demonstrated that nickel-modified montmorillonite effectively reduces the initial cracking temperature of kerogen and enhances the hydrocarbon generation rate. The results of thermogravimetric-Fourier transform infrared spectrum and thermogravimetric-mass spectrometry analysis revealed a significant boost in the production of smaller molecules and non-condensable gases, including hydrogen, methane, ethane, and benzene. Concurrently, there was a notable reduction in carbon dioxide and sulfur dioxide emissions. Pyrolysis experiments were conducted to provide additional evidence of the effectiveness of nickel-modified montmorillonite, confirmed by a decrease in semi-coke production and a notable 11.25% increase in oil yield. Furthermore, the composition analysis of shale oil indicated an increased production of alkenes and aromatic hydrocarbons. These findings suggest that the addition of nickel-modified montmorillonite effectively enhances the depolymerization, deoxygenation and aromatization reaction, resulting in the formation of valuable products during the pyrolysis of oil shale kerogen. This study offers a promising avenue of cost-effective and efficient in-situ oil shale exploitation.

1. Introduction

Oil shale is a type of clay sedimentary rock that is rich in kerogen and can be converted into shale oil through low-temperature pyrolysis (Demirbas, 2016). Abundant oil shale resources can be found in several countries like China (Külaots et al., 2010), Estonia (Gavrilova et al., 2010), Jordan (Al-Jaraden et al., 2023), among others. When effectively developed, this resource can supplement crude oil supplies and enhance energy security. As an unconventional resource type, oil shale holds significant potential for oil and gas development. However, compared to conventional oil resources, its exploitation on an industrial scale faces significant challenges in terms of cost and environmental impacts (Nei et al., 2009; Raukas and Punning, 2009). In line with the current global trend towards the clean development of fossil energy, pursuing in-situ exploitation of oil shale should be considered a viable direction (Ramsay, 2021).

Over the past century, various technologies, such as True In Situ, Modified In Situ, In-situ Conversion Process, ElectrofracTM, Radio Frequency, and Autothermic Pyrolysis, have been invented for in-situ oil shale exploitation (Kang et

Yandy Scientific Press

*Corresponding author.
E-mail address: gujj12138@163.com (J. Gu); denghua13@163.com (S. Deng); syh@cugb.edu.cn (Y. Sun); guowei6981@jlu.edu.cn (W. Guo); chenhan2420@mails.jlu.edu.cn (H. Chen); shiby2420@mails.jlu.edu.cn (B. Shi).

Received December 7, 2023; revised December 30, 2023; accepted January 20, 2024; available online January 25, 2024.

al., 2020a; Ramsay, 2020, 2021; Aurela et al., 2021; Kalu et al., 2022). Nonetheless, these technologies face significant obstacles such as technical difficulties and high development costs, hindering their widespread adoption (Wang et al., 2019; Kang et al., 2020b). In fact, cost reduction and efficiency improvement are crucial elements for the successful commercialization of any in-situ oil shale exploitation technology. Catalytic pyrolysis is considered to be one of the most effective measures: Effective catalysts can significantly reduce the activation energy required for kerogen cracking, thereby increasing the conversion efficiency and improving the quality of oil products.

Traditional efficiency catalysts, such as zeolite (Williams and Chishti, 2001; Park et al., 2021), molecular sieves (Ballice, 2005; Choi et al., 2024), and mineral catalysts (Soerensen and Cant, 1988; Berthonneau et al., 2016; Faisal et al., 2020), have been demonstrated to effectively catalyze the pyrolysis of oil shale. However, implementing these solid-phase catalysts in engineering applications in tight oil shale reservoirs is extremely challenging. In contrast, water-soluble or diffused catalysts are considered more feasible under such conditions.

Some reservoir authigenic minerals, especially clays, have been found to enhance hydrocarbon production and conversion during oil shale pyrolysis (Alstadt et al., 2012; Alves et al., 2020; Lawal et al., 2021). Rahman et al. (2018a) and Lewan et al. (2014) confirmed that montmorillonite (MMT) exhibits physical adsorption and catalytic cracking effects during oil shale pyrolysis, which accelerates decarboxylation and the generation of alkanes.

The catalytic activity of MMT is primarily influenced by its adsorption capacity, ion exchange capacity, and the presence of Lewis and Bronsted acid sites on its surface (Ariskina et al., 2020). The Lewis acid sites of MMT accept electrons, leading to the breakdown of carboxylic acid and the formation of shorter hydrocarbons. These sites have a significant catalytic effect on aromatization (Faure et al., 2006). On the other hand, Bronsted acid sites provide protons to the adsorbed organic matter, catalyzing the conversion of long-chain aliphatic hydrocarbons into shorter ones. MMT also contains alkaline sites, such as Mg^{2+}, which can serve as active centers for the decarboxylation of oxygen-containing molecules. This property of MMT plays a crucial role in facilitating the deoxygenation process in shale oil.

The surface acidity characteristics and catalytic activity of clay minerals can be regulated by altering the surface-adsorbed cations. Thus, by adsorbing suitable catalytically active metal particles, the catalytic cracking of organic matter can be significantly enhanced. Metal salt solutions are commonly used to modify clay minerals because of their strong catalytic activity (Novikau et al., 2022). Metal ions alter the configuration and distribution of electrons on the kerogen surface, accelerating the charge transfer rate between C-C bonds, which leads to the cracking of the kerogen molecule. For instance, MMT modified with cobalt has been shown to improve the pyrolysis characteristics of oil shale and the generation of small molecules (Jiang et al., 2020). Furthermore, nickel-based catalysts have received extensive attention in hydrogenation and dehydrogenation reactions of biomass oil and oil shale due to their good catalytic performance and low cost (Rahman et al., 2018b). However, the application of nickel-modified MMT (Ni-MMT) in catalytic pyrolysis for oil shale remains an unexplored alternative. Using Ni-MMT as a catalyst could minimize interference from other minerals during the pyrolysis process, allowing for a more objective analysis of its impact on oil shale pyrolysis, and provide a theoretical basis for the development of composite catalysts.

Table 1. Ultimate analysis of Huadian oil shale kerogen sample.

Element	Content (dry basis, %)
Carbon (C)	74.68
Hydrogen (H)	9.11
Nitrogen (N)	0.68
HOxygen (O)	13.32
Sulfur (S)	2.21

This study introduces a novel approach for the in-situ exploitation of oil shale by utilizing modified reservoir clay minerals as catalysts. With Huadian oil shale as the research subject, to enhance the catalytic activity of the authigenic clay minerals in oil shale, MMT is modified by introducing acidic sites using nickel. The pyrolysis characteristics of Huadian oil shale kerogen, both with and without the catalyst, are comprehensively analyzed through thermogravimetric (TG) and pyrolysis experiments. Furthermore, the catalytic pyrolysis mechanism of Ni-MMT on kerogen is elucidated, providing valuable theoretical support for the advancement of in-situ oil shale exploitation technologies.

2. Material and methods

2.1 Sample preparation

2.1.1 Kerogen preparation

The kerogen was separated and purified from the oil shale obtained from Huadian, Songliao Basin, China, according to the Chinese National Standard (GB/T 19144-2010). The ultimate analysis results of a kerogen sample are displayed in Table 1.

2.1.2 Synthesis and characterization of Ni-MMT catalyst

The MMT used in this study was sourced from Shandong, China. Chemicals such as NaOH (AR, 99%), Na_2CO_3 (AR, 99%), and $NiCl_2$ (AR, 99%) were purchased from the Beijing Chemical Plant (Beijing, China). The process for modifying clay, crucial for in-situ oil shale exploitation, was carefully designed. The raw MMT was initially purified with sodium carbonate to remove adsorbed calcium ions. A sufficient volume of sodium carbonate solution was added to the MMT suspension, followed by vigorous stirring in a 60 °C water bath. The mixture was then centrifuged repeatedly (3-5 times) and dried to form Na-MMT.

Subsequently, 20 g of Na-MMT was dispersed in deionized water by stirring and ultrasonic treatment, followed by the

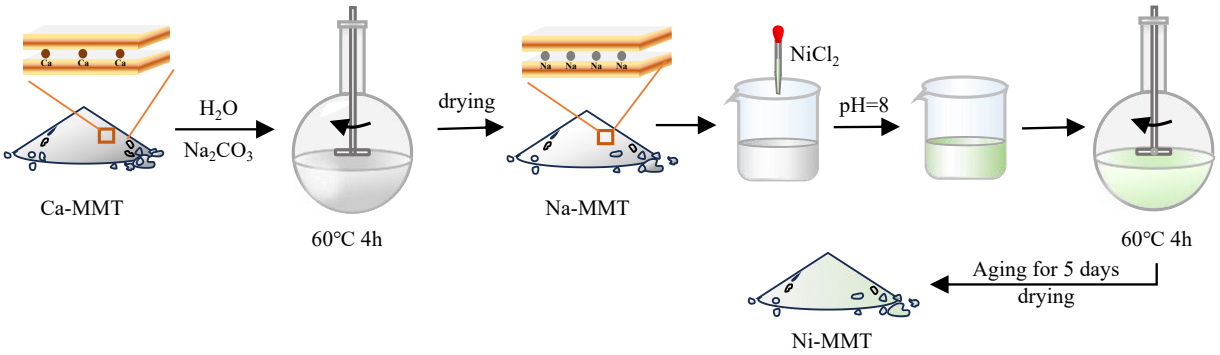

Fig. 1. Preparation process of modified MMT.

incremental addition of 20 mL of 1 mol/L nickel chloride solution. The pH was then adjusted to 8 using 1 mol/L NaOH, and the mixture was stirred for 4 hours in a 60 °C water bath. After 5 days of aging at room temperature, the sample was dried at 60 °C and crushed to a fine powder with 0.18 mm particle size, yielding the Ni-MMT. The detailed preparation process of Ni-MMT is shown in Fig. 1.

Considering the approximate 1:1 ratio of kerogen to MMT in Huadian oil shale samples (Kattai and Lokk, 1998; Razvigorova et al., 2008), we conducted experiments using this ratio to explore the effect of Ni-MMT on the cracking of kerogen. The procedure entailed accurately measuring 10.50 g of both kerogen and modified MMT powder, followed by thorough blending and grinding in a mortar. This grinding process is crucial for achieving a homogenous mixture and ensuring effective contact between the kerogen and the clay mineral, given that kerogen is typically tightly adsorbed within the oil shale matrix.

Field Emission Scanning Electron Microscopy (FE-SEM) and energy dispersion spectroscopy (EDS) were used to observe the structural and morphological changes in MMT following the addition of sodium carbonate and performing nickel modification. The FE-SEM analysis was carried out on a JSM-6700F instrument (JEOL, Japan) equipped with an INCA-SIGHT EDS analysis unit. An acceleration voltage of 8 kV was used for capturing the images, while a voltage of 15 kV was utilized for conducting the analysis. The SEM and EDS results are presented in Fig. 2.

From the SEM photos in Fig. 2, it is evident that the particle size of MMT gradually increases after sodium and nickel modification. This could be attributed to the aggregation of MMT particles during the drying process after sodium modification. Subsequently, when the MMT was further modified with nickel, the aggregation phenomenon was exacerbated due to the stronger interlayer adsorption of nickel ions on MMT.

The EDS results shown in the histogram of Fig. 2(d) confirm the successful incorporation of sodium and nickel into the MMT and Na-MMT interlayer, with respective contents of 3.1% and 2.1%. Additionally, the EDS analysis of Ni-MMT reveals that calcium ions are present, which can be attributed to the fact that although calcium ions adsorbed on the surface and interlayer of natural MMT precipitate as calcium carbonate during the sodium modification process, they become mixed with the MMT in solid form after drying, and calcium carbonate is therefore also retained in Ni-MMT. However, its content is very low and its interaction with MMT is minimal, exerting a negligible influence on the catalytic pyrolysis process of organics.

2.2 Pyrolysis experiments of kerogen with catalysts

Pyrolysis experiments of kerogen with/without catalysts were carried out in a modified Fisher assay analyzer (Guo et al., 2023). About 10.00 g of kerogen with/without modified MMT was placed into the center of a quartz glass reactor. Nitrogen was then vented into the reactor at a flow rate of 50 mL/min for 5 minutes to maintain an oxygen-deficient atmosphere. The reaction was heated at a rate of 10 °C/min until reaching 520 °C, which was held for 10 minutes. The produced shale oil and semi-coke were collected separately. The oil yield was calculated according to the following formula:

$$\varphi = \frac{m_0}{m_k} \times 100\% \tag{1}$$

where m_0 (g) represents the shale oil mass of kerogen produced, m_k (g) represents the mass of the kerogen sample, and φ (%) represents the oil yield of kerogen.

2.3 Thermogravimetry-Fourier transform infrared spectroscopy (TG-FTIR)

In order to evaluate the thermal behavior and nature of evolved gases from sample pyrolysis, TG-FTIR analysis was conducted using a TG analyzer (STA 499 F3, Netzsch Company, Germany) coupled with a Fourier transform infrared (FTIR) spectrometer (Nicolet iS10, Thermo Electron, America). To ensure the efficient transfer of volatiles from the TG analyzer to the FTIR spectrometer, a 1 m long Teflon tube with an internal diameter of 2 mm was connected. The transfer line was heated to and maintained at a constant temperature of 200 °C to prevent gas condensation during the TG-FTIR analysis. The absorbance spectra of the evolved gases were recorded at a frequency of 8 times per minute by the spectrometer. The measurements were taken within the wavenumber range of 4,000-400 cm^{-1}. For each run, about 10 mg of sample was heated from 30 to 800 °C at a rate of 10 °C/min. Nitrogen was used as the carrier gas at a flow rate of 60 mL/min during

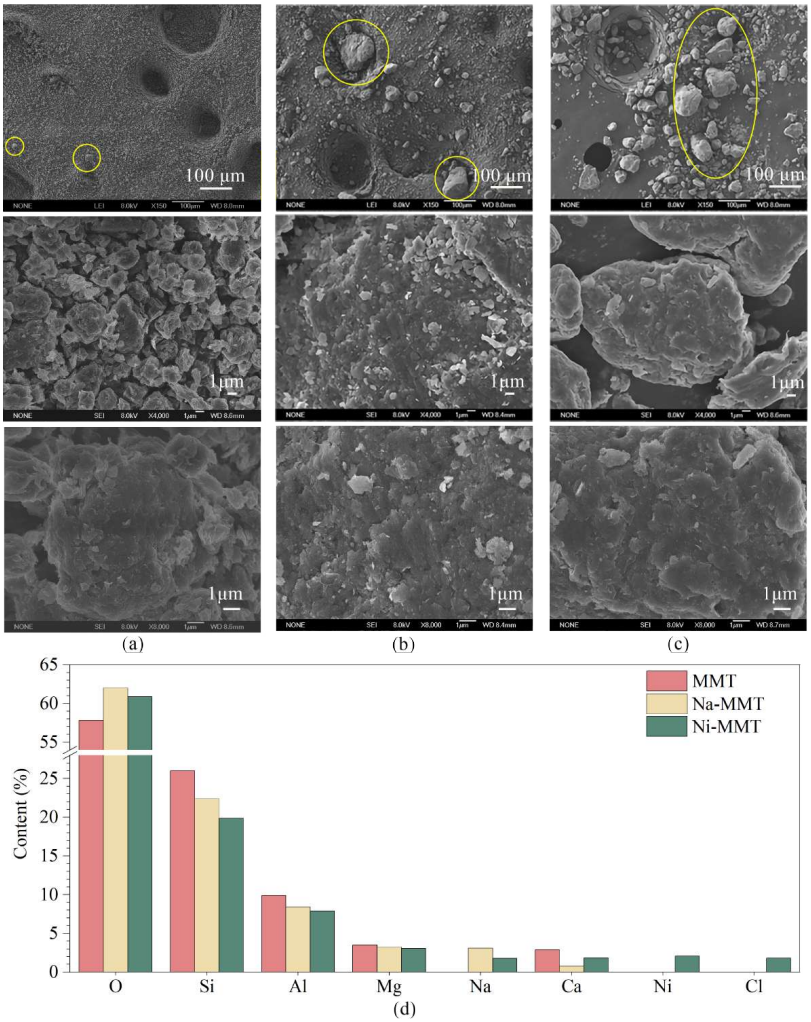

Fig. 2. SEM images and EDS analysis of the MMT surface. (a) MMT, (b) Na-MMT, (c) Ni-MMT and (d) EDS analysis.

the TG-FTIR experiment.

2.4 Thermogravimetry-mass spectrometry (TG-MS)

The TG-MS test of the samples was performed using a NETZSCH STA449F3 QMS403D thermogravimetry analyzer coupled with a Bruker V70 mass spectrometer. The thermally degenerated gas was recorded by mass spectrometry online detection. For each run, approximately 30 mg of sample was heated from 40 to 800 °C at a rate of 10 °C/min under a nitrogen atmosphere.

2.5 Gas chromatography-mass spectrometry (GC-MS)

The composition of shale oil obtained from the Fisher assay analysis was determined using GC-MS technology. This was achieved by using an Agilent 7890A-5975N system equipped with an HP-5MS capillary column (30 m × 0.32 mm × 0.25 μm). Helium was the carrier gas, and the analysis was performed in constant current mode with a flow rate of 2 mL/min and a split ratio of 50:1. The column temperature was initially set at 50 °C and held isothermally for 5 min. Subsequently, the temperature was increased at a rate of 10 °C/min up to 280 °C and held for 12 minutes. Two injections were performed for each sample to ensure accuracy and reproducibility. Compound detection was carried out according to the National Institute of Standards and Technology mass spectrometry library (Version 2.02) as the reference database.

3. Results and discussion

3.1 Catalytic pyrolysis behavior of kerogen

The catalytic pyrolysis behavior of kerogen is crucial regarding its decomposition mechanism. TG can effectively measure the mass loss of a substance as a function of temperature, providing insights into different stages of kerogen pyrolysis. The TG and derivative thermogravimetric (DTG) curves show these stages for kerogen with/without catalysts in Fig. 3. The TG results reveal that the mass loss during kerogen pyrolysis involves dehydration and decomposition processes. Since the drying process after MMT modification was carried out at a lower temperature, dehydration peaks indicating interlayer water release are found near 100 °C on

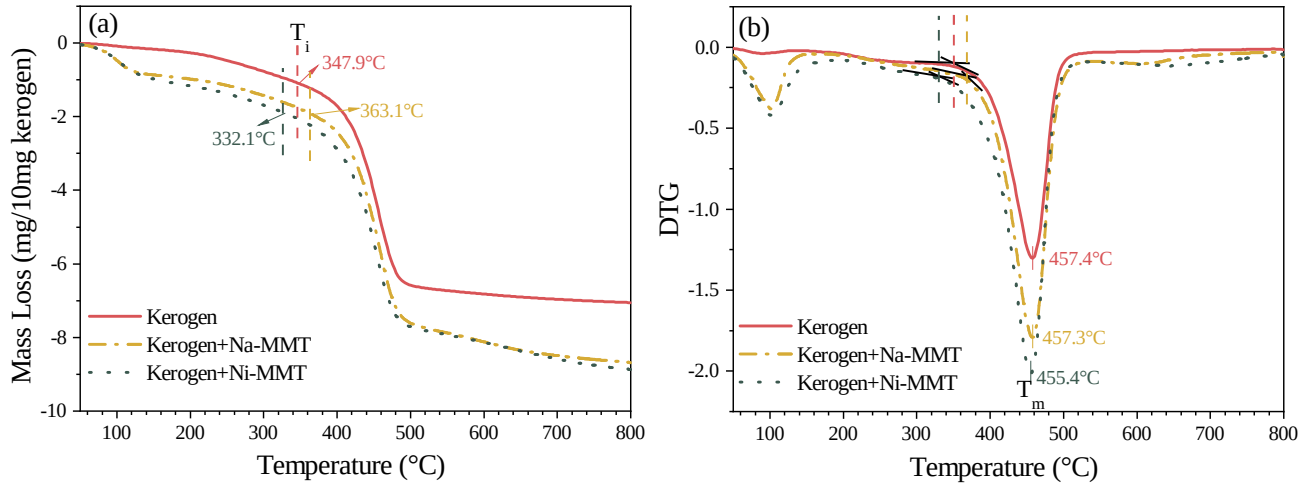

Fig. 3. (a) TG and (b) DTG curves of kerogen with/without modified MMT.

Table 2. Ultimate analysis of Huadian oil shale kerogen sample.

Sample	T_i (°C)	T_t (°C)	T_m (°C)
Kerogen	347.9	480.2	457.7
Kerogen+Na-MMT	363.1	480.1	457.7
Kerogen+Ni-MMT	332.1	475.7	455.4

the DTG curves of both MMT-containing samples. This dehydration behavior of MMT does not have any detrimental effect on the cracking of organic matter. Therefore, subsequent analyses were primarily focused on the decomposition process of organic matter.

The DTG curve exhibits a single peak attributed to the pyrolysis of kerogen at 400-550 °C, reflecting a concentrated decomposition phase within this temperature range. In fact, the pyrolysis of kerogen undergoes several stages. Kerogen is initially decomposed into pre-asphaltene, which is a complex mixture of high molecular weight compounds. Subsequently, it undergoes depolymerization and further decomposition at higher temperatures and is gradually released in a gaseous form.

The initial pyrolysis temperature (T_i), the termination temperature (T_t), and the temperature corresponding to the maximum rate of mass loss (T_m) were determined based on the DTG curves presented in Table 2. These temperatures are crucial in understanding the behavior of kerogen during pyrolysis and the influence of the catalyst. Notably, there is a right shift in Ti from 348 to 363 °C during the pyrolysis of kerogen with Na-MMT. This shift can be attributed to the adsorption of organic matter by MMT, inhibiting the release of some free organics and weakly bonded kerogen fragments at the initial pyrolysis stage. Conversely, using Ni-MMT as a catalyst significantly reduces the T_i, suggesting that the surface of Ni-MMT, rich in Lewis acid centers, effectively enhancing the cleavage of kerogen-derived organics such as pre-asphaltene and asphaltene. In comparison, the introduction of two types of MMT has no discernible influence on T_t and T_m. This observation suggests that MMT has limited influence on the chemical reactions that occur in kerogen during the later stages of maturation at high temperatures.

3.2 Characteristics of gas release during the catalytic pyrolysis of kerogen

3.2.1 TG-FTIR analysis

In-situ infrared analysis was conducted to evaluate the composition of volatile compounds generated during the thermal decomposition process of kerogen. The three-dimensional (3D) TG-FTIR spectra of gaseous products of the pyrolysis of kerogen with/without catalysts are presented in Fig. 4. The FTIR characteristic absorption bonds for various gases and functional groups in the gaseous products were summarized based on previously reported data (Braun et al., 2007), with the results shown in Table 3. The main gas products observed are CH_4, CO_2, CO, and SO_2, while the typical functional groups of gas-phase molecules include C-H, C=O, C=C, and S=O.

As can be seen from the 3D diagrams in Fig. 4, a remarkable pair of bimodal peaks attributed to C-H stretching vibration appear in the 3,000-2,850 cm^{-1} wavenumber range and the 400-550 °C temperature range (Shi et al., 2024). This is indicative of a substantial production of aliphatic compounds, which are the main components of kerogen matter. It is worth noting that the bond at 3,017 cm^{-1} is considered as the characteristic absorption bond of CH_4. The formation of methane is mainly attributed to the decomposition of methoxy groups and the cracking of methyl-containing aliphatic or aromatic side chains (Bai et al., 2019). The bands at 2,400-2240 cm^{-1} and 740-600 cm^{-1} are characteristic peaks of CO_2. The generation of CO_2 is mainly attributed to the cracking and reformation of heterocyclic oxygen or carboxyl, carbonyl and carboxylic functional groups in the organic compounds (Lorant et al., 2008). Some CO appearing at 2,240-2,060 cm^{-1} is likely formed through the decomposition of molecules containing C-O-C and C=O functional groups. The peaks at 1,420-1,300 cm^{-1} can be assigned to the S=O vibration in some organic sulfur-oxygen compounds, such as sulfones and sulfoxides. In

Table 3. FTIR characteristic absorption bands of kerogen pyrolyzates.

Gaseous product or functional group	Structure	Wavenumber (cm^{-1})
CH_4	Non-condensable gas	3,017
CO_2	Non-condensable gas	2,400-2,240, 740-600
CO	Non-condensable gas	2,240-2,060
SO_2	Non-condensable gas	1,374
O-H stretching vibration	Water	4,000-3,500
C-H stretching vibration	Methyl, methylene	2,970-2,890
	aryl-methyl	2,858
C=O stretching vibration	Carbonyl compounds: ketone, acid, acetate, ester, aldehyde	1,850∼1,600
C=C stretching vibration	Aromatic compounds	1,600-1,420
S=O stretching vibration	Sulfones, sulfoxides, etc.	1,420-1,300
C-H bending vibration	Saturated aliphatic hydrocarbons	960-912

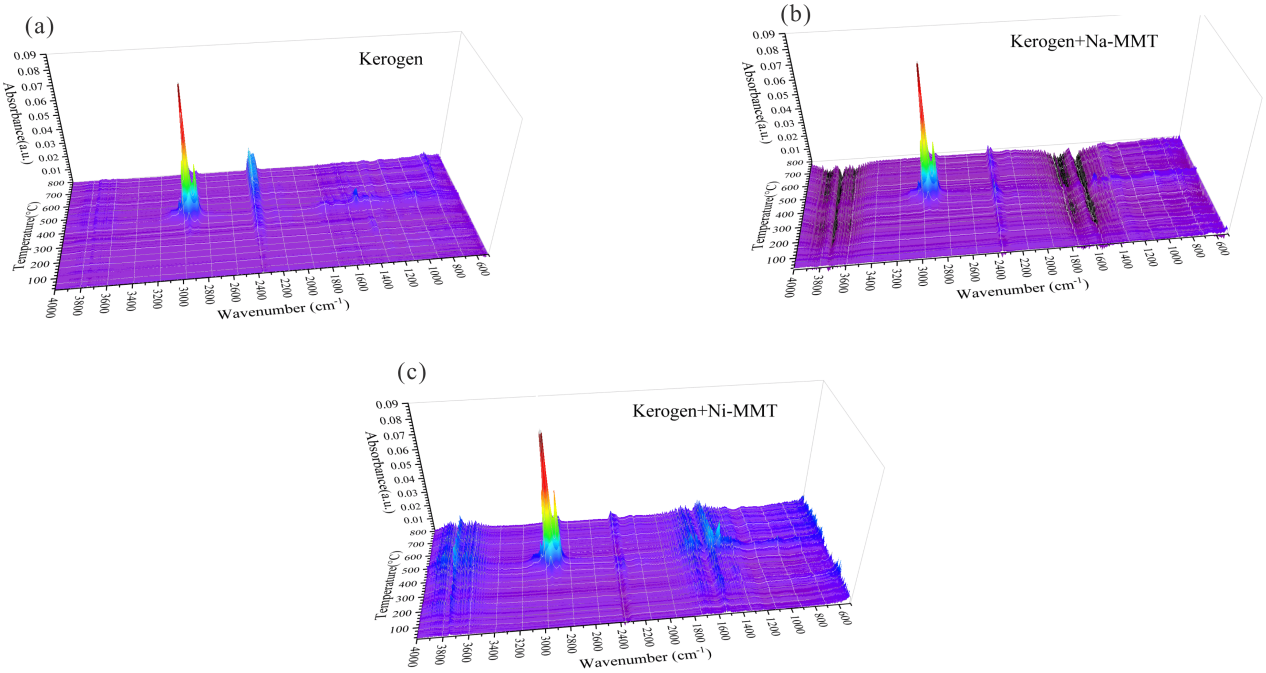

Fig. 4. 3D TG-FTIR diagrams of pyrolysis gaseous product of (a) kerogen, (b) kerogen+Na-MMT and (c) kerogen+Ni-MMT.

particular, the band at 1,374 cm^{-1} is likely a characteristic peak of SO_2.

In order to meticulously analyze the evolution characteristics of non-condensable gas during pyrolysis, the absorbance data of the pyrolysis gas from kerogen with/without catalysts at the same wavenumber (CH_4, 3,017 cm^{-1}; CO_2, 2,360 cm^{-1}; CO, 2,180 cm^{-1}; SO_2, 1,374 cm^{-1}) were extracted from Fig. 4 and plotted in Fig. 5. The impact of catalyst on the gas content can be compared by calculating the peak area in the spectrum, and the corresponding results are shown in Table 4.

Firstly, as can be observed in Fig. 5(a), during the pyrolysis process of kerogen, the generation of CH_4 exhibits a distinct parabolic pattern focused in the temperature range of 400-600 °C. This phase corresponds to the primary pyrolysis of kerogen organics, in which numerous carbon chains of aliphatics and side chains aromatics undergo decomposition, leading to CH_4 production. The results of peak area analysis in Table 4 indicate that the introduction of Na-MMT inhibits the generation of CH_4 from kerogen pyrolysis, while that of Ni-MMT promotes it. This can be attributed to the adsorption of certain kerogen-derived organics in the layers or on the surface of MMT, which may result in a decrease in CH_4 release after the introduction of Na-MMT. Conversely, Ni-MMT has higher acid activity and can facilitate the pyrolysis of these adsorbed organics, thereby increasing CH_4 production.

Secondly, two absorption peaks of CO_2 can be found in

Table 4. Peak wavenumber and area of non-condensable gas in the FTIR spectrum.

Wavenumber (cm^{-1})	Non-condensable gas	Sample	Peak 1		Peak 2	
			Center	Area	Center	Area
3,017	CH_4	Kerogen	470	0.9796	-	-
		Kerogen+Na-MMT	473.33	0.8430	-	-
		Kerogen+Ni-MMT	473.33	1.0582	-	-
2,360	CO_2	Kerogen	430	0.9290	757	4.3778
		Kerogen+Na-MMT	410	1.50662	653	1.7301
		Kerogen+Ni-MMT	380	0.8011	643	1.3931
2,180	CO	Kerogen	433	0.1855	603	0.2329
		Kerogen+Na-MMT	420	0.3097	730	0.2624
		Kerogen+Ni-MMT	430	0.2244	707	0.5235
1,374	SO_2	Kerogen	287	0.2533	-	-
		Kerogen+Na-MMT	263	0.1411	-	-
		Kerogen+Ni-MMT	300	0.1114	-	-

the infrared spectrum, as shown in Fig. 5(b). The first peak appears between 300 and 500 °C, mainly due to the cracking of organic matter containing oxygen-containing functional groups (Ritchie et al., 1985; Pan et al., 2016). The relative subtleness of this peak suggests a limited presence of such groups in kerogen, possibly influenced by acid washing and demineralization during preparation. The second CO_2 absorption peak appears at a higher temperature, possibly due to CO_2 production during the condensation reaction of polycyclic aromatic compounds. After adding MMT, both peaks decrease significantly, with the second peak nearly disappearing. This could be because oxygen-containing functional groups in organic matter are easily adsorbed on the surface of clay minerals, resulting in a considerable decrease in CO_2 emissions following kerogen cracking. Compared to Ni-MMT, Na-MMT exhibits a more pronounced reduction in CO_2 production. This difference in performance can be attributed to the higher catalytic activity of nickel, which facilitates the cracking and removal of certain functional groups.

Thirdly, the formation of CO during kerogen pyrolysis with/without catalysts is depicted in Fig. 5(c). CO is mainly formed via the decarboxylation and cleavage of ether bonds from the kerogen fragments. The spectra indicate that modified MMT, especially at temperatures above 550 °C, significantly promotes CO formation compared to kerogen pyrolysis alone. This means that the Lewis acid sites on the surface of MMT are involved in the reaction, contributing to the decomposition of oxygenated molecules containing C-O-C and C=O functional groups (Zhang et al., 2022). Also, the presence of nickel appears to enhance the reduction reaction of CO_2 into CO at higher temperatures.

Finally, as seen in Fig. 5(d), the spectra of kerogen cracking gas exhibit two absorption peaks corresponding to 1,374 cm^{-1}. The first peak of SO_2 appears at 220-360 °C, which is ascribed to the decomposition of pyrite (Ibarra et al., 1989). Another peak may correspond to the C-H stretching vibration. Notably, the addition of modified MMT, particularly Ni-MMT, seems to inhibit the decomposition of pyrite, possibly due to its active sites and adsorption properties.

Based on the characteristic temperatures T_i, T_t and T_m obtained from the T_G analysis in Table 2, the infrared spectra of the pyrolysis gas from kerogen at 360, 450 and 500 °C were extracted from the 3D FTIR diagrams in Fig. 4, and shown in Fig. 6. Compared to Fig. 5, Fig. 6 provides a clearer demonstration of changes in the pyrolysis reaction of kerogen after the addition of MMT catalysts at these temperatures.

At 360 °C, the highest absorption intensity is observed for CO_2, followed by CH_4, while other gases and functional group products are not produced in significant amounts. It can be observed that the release of CO_2 is reduced after adding MMT. When the temperature reaches 450 °C, the intensity of the C-H stretching vibration absorption peak increases and it becomes the highest peak. This change, especially accentuated after introducing the catalysts, indicates an increased abundance of C-H bonds. The presence of modified MMT seems to facilitate the free-radical reactions of organic matter, thus promoting the generation of aliphatic hydrocarbons. At the termination temperature of 500 °C, due to the hysteresis effect of the infrared results, the C-H bond peak exhibits a sustained high intensity in Ni-MMT catalyzed kerogen decomposition. This observation further suggests that the presence of Ni-MMT promotes the more thorough cracking of kerogen.

3.2.2 TG-MS analysis

The changes in volatile products resulting from the thermal decomposition of Huadian kerogen under the catalysis of mod-

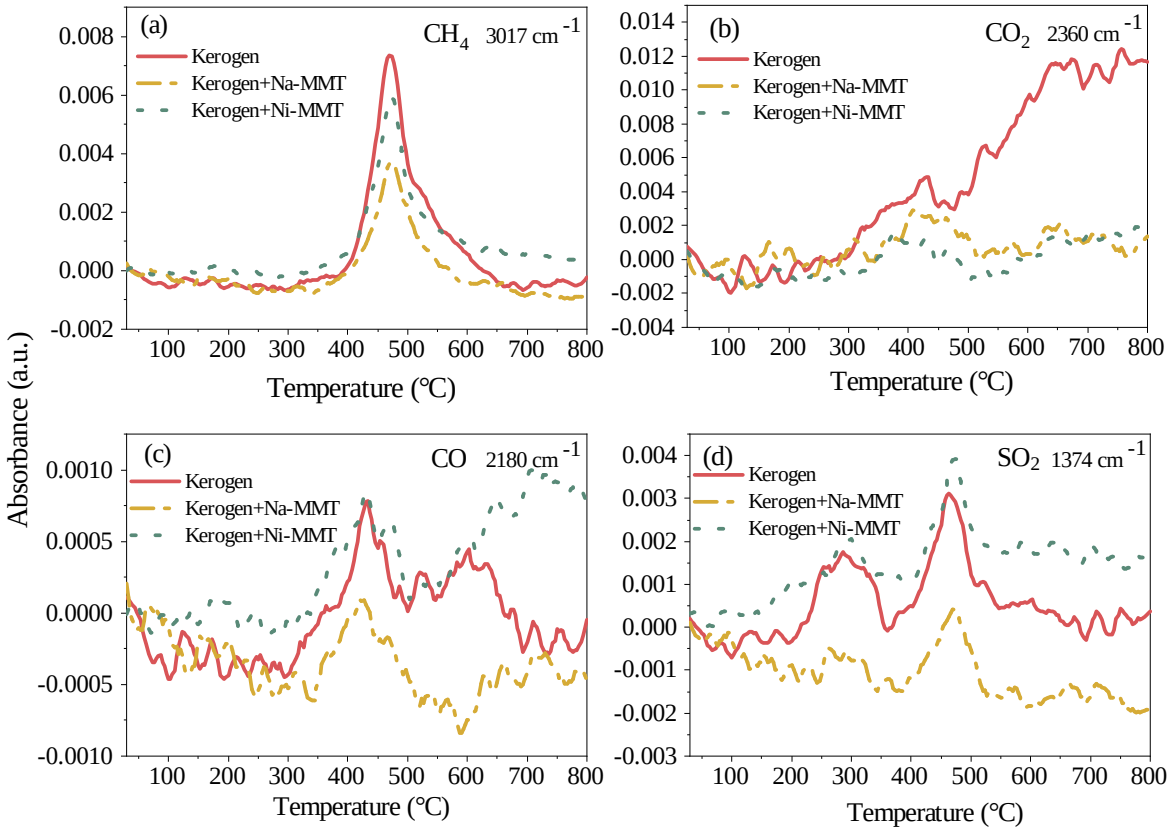

Fig. 5. Effect of temperature on the evolution characteristics of non-condensable gas. (a) CH_4, 3,017 cm^{-1}, (b) CO_2, 2,360 cm^{-1}, (c) CO, 2,180 cm^{-1} and (d) SO_2, 1,374 cm^{-1}.

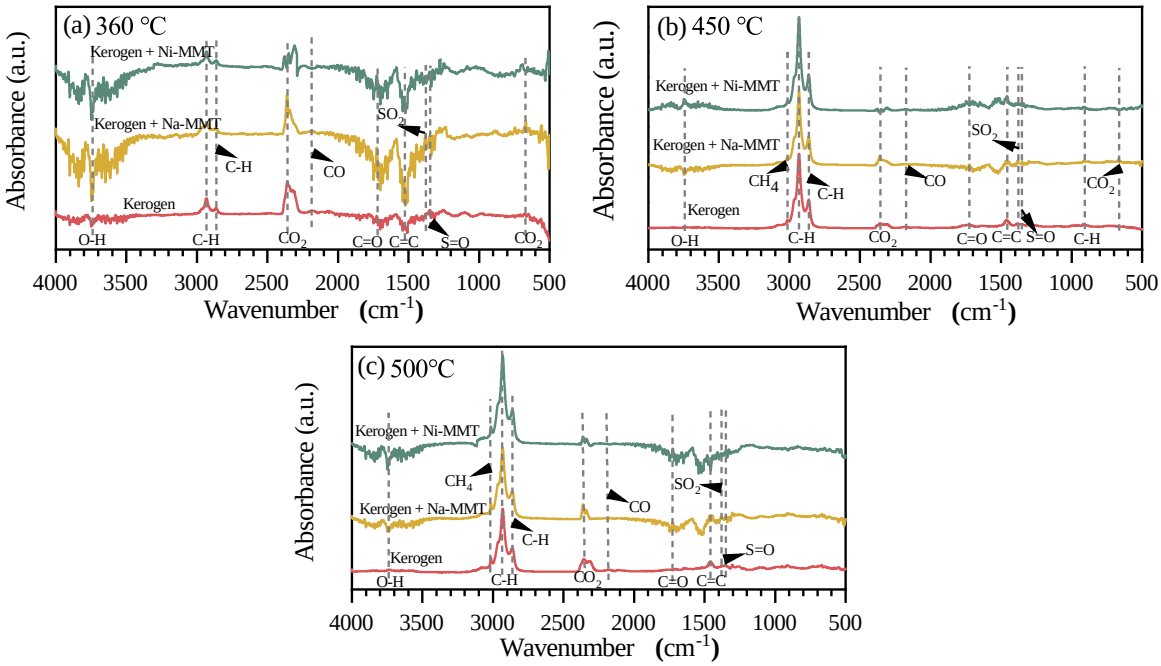

Fig. 6. FTIR spectra of pyrolysis product evolving from kerogen with/without modified MMT at (a) 360 °C, (b) 450 °C and (c) 500 °C.

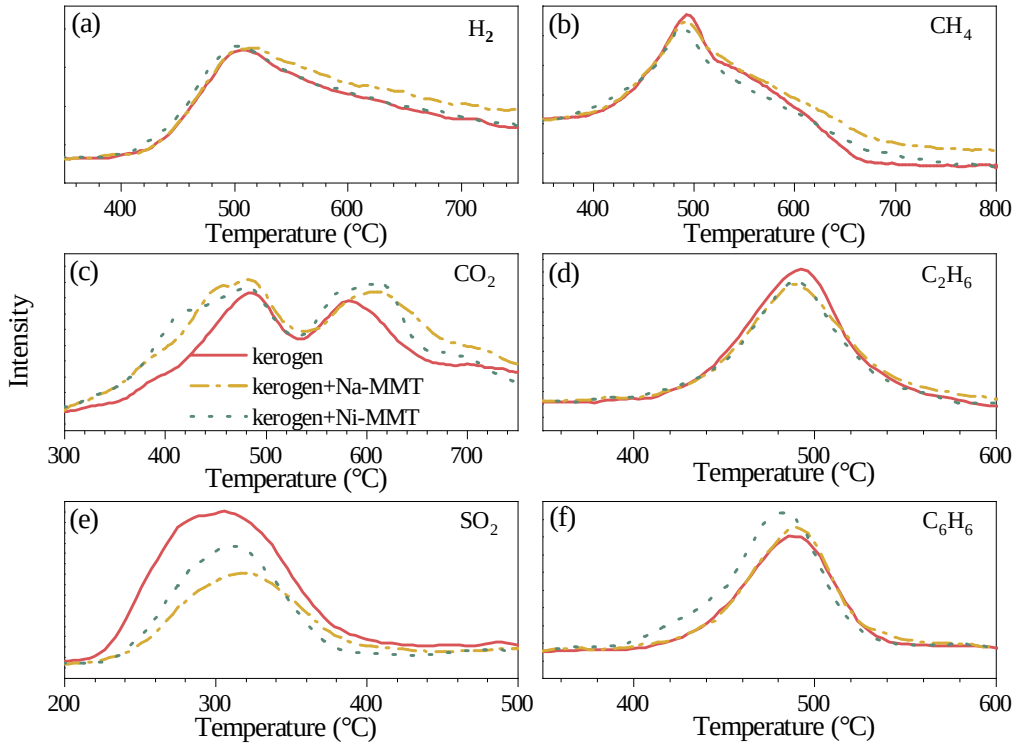

Fig. 7. Ion current signal intensity curves of (a) H_2, (b) CH_4, (c) CO_2, (d) C_2H_6, (e) SO_2, and (f) C_6H_6 during kerogen pyrolysis with/without modified MMT.

ified MMT were further investigated using TG-MS analysis. Thus, we aimed to further explore the pyrolysis pathways of kerogen under the influence of catalysts. The observed types of hydrocarbon compounds observed included alkanes, alkenes, alkynes, cyclic compounds, and aromatics. The detected non-hydrocarbon compounds included H_2, H_2S, H_2O, CO, CO_2 and SO_2. Fig. 7 shows the evolution curves of hydrogen (m/z = 2), CO_2 (m/z = 44), SO_2 (m/z = 64), methane (m/z = 16), ethane (m/z = 30), and benzene (m/z = 78) before and after the addition of modified MMT during kerogen pyrolysis.

The hydrogen evolution curves during the pyrolysis of each sample indicate a wide temperature range for hydrogen generation. Hydrogen emission begins at 400 °C, initially increases and then decreases, and peaks around 500 °C. Hydrogen is primarily generated through polycondensation between free radicals and the dehydrogenation of the aromatic lamellar structure after the release of aliphatic kerogen fragments (Campbell, 1978; Li et al., 2017). The introduction of Ni-MMT accelerates the release of hydrogen, suggesting its catalytic effect on the dehydrogenation reaction. In contrast, Na-MMT appears to delay hydrogen release at elevated temperatures. In terms of CO_2 emission, the release curve exhibits a clear bimodal structure. The first peak is mainly attributed to the cracking of carboxyl, carbonyl and carboxylic functional groups, while the second peak is caused by the condensation reactions of aromatic compounds. The addition of MMT promotes the cleavage of these chemical bonds in organic matter, leading to an increase in CO_2 release. This finding is consistent with the results of TG-FTIR analysis. Furthermore, as shown in Fig. 7, the release of SO_2 is influenced by MMT, with the acid sites on its surface adsorbing the gas, leading to a notable decrease in its release.

In the upper right picture in Fig. 7, methane generation can be observed during kerogen pyrolysis with/without MMT as catalysts. As depicted in the figure, methane production begins at about 400 °C, peaks at around 500 °C, and subsequently declines until it ceases at approximately 650 °C. Methane generation can be divided into three stages: (1) CH_4 is mainly formed through the cracking of long-chained aromatic groups-alkyl groups-ether bonds at 400-460 °C; (2) at temperatures between 460 and 555 °C, CH_4 is produced through the secondary cleavage of long-chain alkanes; (3) from 550 to 700 °C, CH_4 is generated through condensation reactions of aromatic molecules (Cui et al., 2023). The inclusion of MMT has a minimal impact on CH_4 formation. With the addition of catalysts, the release of CH_4 is slightly accelerated. The peak temperature of CH_4 release is reduced from 496 to 489 °C when Ni-MMT is used as the catalyst.

The generation of ethane is primarily attributed to the decomposition of macromolecular compounds in the kerogen structure, such as the decomposition of aromatic units, aliphatic bridges, and certain oxygenated polymethylene compounds (Cui et al., 2023). The C_2H_6 generation curves follow a similar trend to that of CH_4 during pyrolysis, but it is concentrated at temperatures ranging from 400 to 580 °C. The addition of MMT leads to a slight decrease in the release of

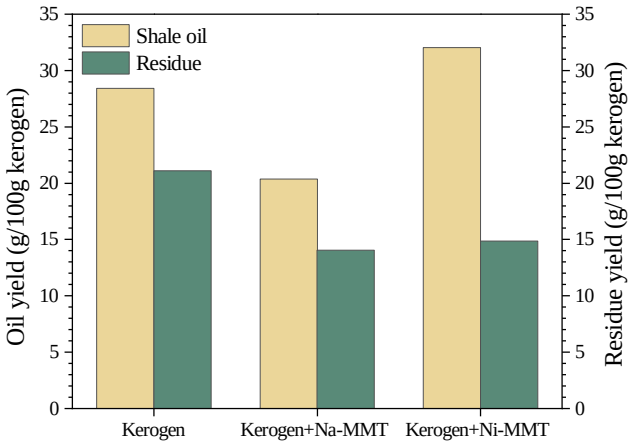

Fig. 8. Effect of modified MMT on shale oil yields.

C_2H_6, which can be attributed to the adsorption of organic matter by MMT. However, the observed effect is not significant.

Aromatics comprise the skeleton of kerogen. As shown in the lower right graph of Fig. 7, the evolution curve of benzene exhibits a symmetrical narrow peak, similar to that of ethane. The peaks near 500 °C are attributed to the breaking of bridge bonds connecting aliphatic chains to the C_6H_6 ring (Sun et al., 2006). MMT is favorable to produce C_6H_6 compounds. Especially, Ni-MMT not only enhances the C_6H_6 yield but also reduces the C_6H_6 generation temperature. This phenomenon can be attributed to the ability of nickel to facilitate the cleavage of bridge bonds connecting aliphatic and benzene rings, as well as condensation and aromatization. The latter reactions will lead to dehydrogenation, increasing the release of hydrogen, in line with the discussion of hydrogen release earlier in this section.

3.3 Characterization of shale oil composition

Fischer assay analysis experiments were conducted on kerogen with modified MMT to further investigate the catalytic mechanism. The yields of shale oil and residue are presented in Fig. 8. Since clay minerals remain stable at this temperature, the residue yields were calculated based on the change in kerogen content: the oil yield from Huadian kerogen was 28.42%. Upon the addition of Na-MMT and Ni-MMT, the oil yield decreased and increased, respectively. However, both catalysts resulted in a reduction in the residue yield, suggesting that the inclusion of a catalyst enhances the thorough decomposition of organic matter. Notably, MMT generates a greater amount of gas, while Ni-MMT promotes the production of shale oil. The adsorption capacity of MMT surface inhibits the release of organic matter between layers, while the catalytic active sites on the surface facilitate the formation of small molecule gases, such as CO_2 and CH_4. Meanwhile, the chemisorption between Ni and H atoms could weaken the C-H bond energy, leading to the formation of hydrogen radicals. These radicals facilitate kerogen cracking, thereby increasing the shale oil yield.

The compositions of shale oil obtained from the pyrolysis of kerogen with/without MMT were determined using a GC-MS analyzer. Fig. 9 displays the total-ion chromatograms of the oil products. From the figure, the similar composition of oil products in the three groups of experiments is obvious: The main compositions of samples are alkanes, alkenes, oxygenates, a small number of aromatics, and iso-hydrocarbon.

The normalized content of the primary constituents of shale oil is depicted in Fig. 10. The main components are n-alkanes and n-alkenes, totaling approximately 90% of the composition. The introduction of MMT leads to a decrease in alkanes and an increase in alkenes, suggesting that MMT may promote the cracking or dehydrogenation process of alkanes. Furthermore, Na-MMT may have a promotive effect on isomerization, since the proportion of iso-hydrocarbons generated during the co-pyrolysis of kerogen with Na MMT slightly increases. The addition of Ni-MMT leads to a reduction in oxygen-containing compounds within shale oil while promoting the generation of aromatic hydrocarbons.

Catalytic pyrolysis reactions involve various processes such as degradation of the macromolecule by chain scission, cyclization, decarboxylation, and aromatization (Dai et al., 2019). In the case of Na-MMT, acid sites on the surface play a crucial role in the cleavage of C-C bonds, rendering catalytic activity that leads to the production of methane, alkenes and cycloalkanes. This catalytic effect is illustrated in Fig. 10, which is manifested in the increased abundance of alkenes and iso-hydrocarbons in shale oil. The Na^+ remains separated within Na-MMT, largely present in the interstitial cavity where it is bound by ionic forces to balance the negative charge of O^-. Yet, some Na^+ are unable to penetrate the interlayer of MMT, resulting in strong charge separation. This phenomenon enhances condensation reactions and promotes the formation of alkenes (Chtourou et al., 2019). Moreover, the presence of nickel in Ni-MMT influences the pyrolysis of organic matter; it facilitates catalytic cracking and enhances the release of organics from kerogen. Consistent with the TG-MS analysis, the Ni-MMT has an elevated content of aromatics; this is due to the robust dehydrogenation activity of nickel, which effectively catalyzes dehydrogenation, cyclization and aromatization reactions. Consequently, there is a noticeable increase in the abundance of aromatic hydrocarbons, as nickel promotes these specific chemical transformations in the kerogen.

From Fig. 9, it is evident that the inclusion of MMT enhances the peak intensity of alkenes in the shale oil spectra. This effect is particularly pronounced in the short-chain hydrocarbon region on the left side of the graph, where the peak representing n-alkenes surpasses the corresponding peak for n-alkanes. To delve deeper into the relationship between n-alkenes and n-alkanes with varying carbon numbers, further investigations were conducted. The results presented in Fig. 11 indicate that Na-MMT, via the influence of Na^+ on the charge separation effect of MMT, promotes the polycondensation reaction of organics, substantially enhancing the radio of alkanes to alkenes. In contrast, as mentioned previously, the interaction between Ni and H atoms in Ni-MMT leads to the cleavage of the C-H bonds and the generation of hydrogen radicals. This dehydrogenation process results in an increased content of alkenes and aromatic hydrocarbons in organic matter.

In summary, the utilization of modified reservoir clay, such

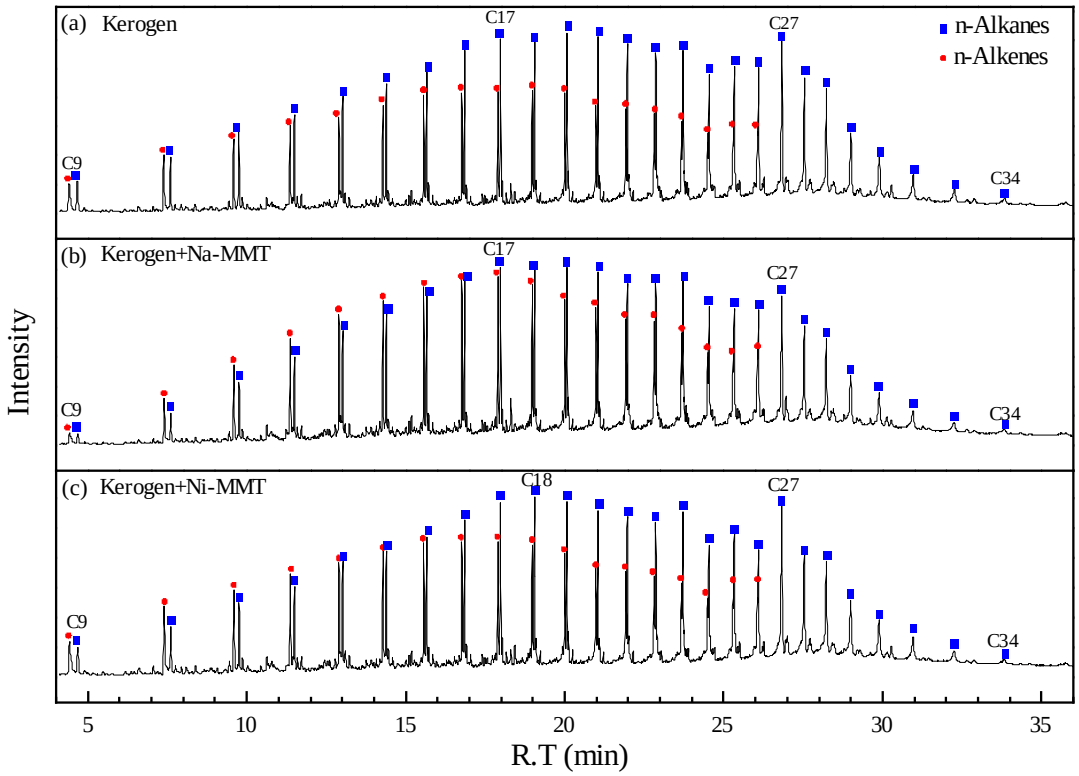

Fig. 9. Gas chromatography-mass spectrum of shale oil obtained from the pyrolysis of (a) kerogen (b) kerogen+Na-MMT and (c) kerogen+Ni-MMT.

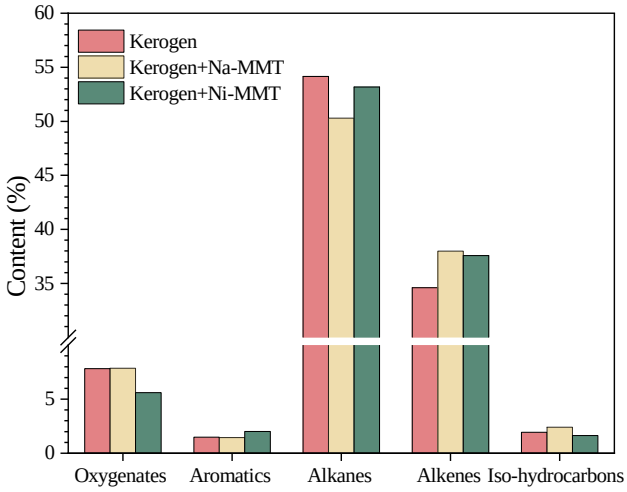

Fig. 10. Composition of shale oil.

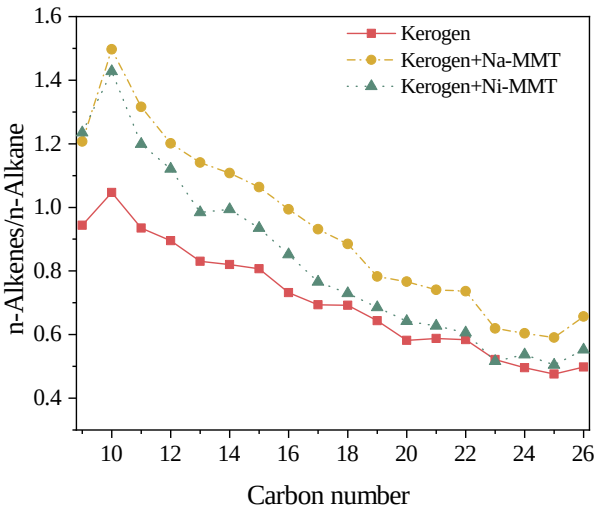

Fig. 11. Relationship between the ratio of n-alkene to n-alkane and carbon number.

as MMT, as a catalyst in the in-situ exploitation of oil shale, enables prolonged contact and more comprehensive reactions between oil and gas products and clay during migration. As such, the incorporation of modified MMT enhances the conversion rate of organic matter. It facilitates catalytic dehydrogenation, leading to a higher alkane content. Consequently, this method holds great potential for reducing costs and enhancing efficiency in the in-situ transformation process of oil shale, providing a valuable approach to optimizing the production of valuable hydrocarbons.

4. Conclusions

We present an innovative approach in the field of oil shale exploitation by employing Ni-MMT as a catalyst for the pyrolysis of kerogen in the Huadian oil shale. The results demonstrate that the incorporation of Ni-MMT significantly lowers the initial pyrolysis temperature of kerogen and enhances hydrocarbon generation. These effects can be attributed to the catalytic activity of nickel, which promotes the

cleavage of kerogen-derived organics, such as pre-asphaltene and asphaltene. Furthermore, a noteworthy 11.25% increase in oil yield could be observed, accompanied by a decrease in semi-coke production, and a significant shift occurred in the composition of shale oil towards higher concentrations of alkenes and aromatic hydrocarbons. The latter is attributed to the chemisorption between Ni and H atoms, which weakens the C-H bond energy and augments dehydrogenation reactions. Importantly, the utilization of Ni-MMT not only improves the yield and quality of shale oil but also contributes to environmental sustainability by reducing the formation of oxygenated compounds, resulting in lower CO_2 and SO_2 emissions.

The application of modified MMT in the in-situ conversion of oil shale represents a highly promising method to enhance pyrolysis efficiency and establishes a groundwork for future investigations on optimizing the modification of reservoir clay minerals. This innovative approach holds great potential for advancing the commercial development of in-situ catalytic pyrolysis technology in oil shale, offering a solution toward more effective and efficient ways of exploitation.

Acknowledgements

This work was supported by the National Key R&D Program of China (No. 2019YFA0705502), and the Young and Middle-aged Excellent Team Project for Scientific and Technological Innovation of Jilin Province (No. 20220508135RC). We also appreciate the reviewers' and editors' constructive comments to make the paper high-quality.

Conflict of interest

The authors declare no competing interest.

References

Al-Jaraden, T., Ayadi, O., Alahmer, A. Towards sustainable shale oil recovery in Jordan: An evaluation of renewable energy sources for in-situ extraction. International Journal of Thermofluids, 2023, 20: 100446.

Alstadt, K. N., Katti, D. R., Katti, K. S. An in situ FTIR step-scan photoacoustic investigation of kerogen and minerals in oil shale. Spectrochimica Acta Part A: Molecular and Biomolecular Spectroscopy, 2012, 89: 105-113.

Alves, J. L., Rosa, P., Realinho, V., et al. The effect of Brazilian organic-modified montmorillonites on the thermal stability and fire performance of organoclay-filled PLA nanocomposites. Applied Clay Science, 2020, 194: 105697.

Ariskina, K. A., Yuan, C., Abaas, M., et al. Catalytic effect of clay rocks as natural catalysts on the combustion of heavy oil. Applied Clay Science, 2020, 193: 105662.

Aurela, M., Mylläri, F., Konist, A., et al. Chemical and physical characterization of oil shale combustion emissions in Estonia. Atmospheric Environment: X, 2021, 12: 100139.

Bai, J., Chen, X., Shao, J., et al. Study of breakage of main covalent bonds during co-pyrolysis of oil shale and alkaline lignin by TG-FTIR integrated analysis. Journal of the Energy Institute, 2019, 92(3): 512-522.

Ballice, L. Effect of demineralization on yield and composition of the volatile products evolved from temperature-programmed pyrolysis of Beypazari (Turkey) Oil Shale. Fuel Processing Technology, 2005, 86(6): 673-690.

Berthonneau, J., Grauby, O., Abuhaikal, M., et al. Evolution of organo-clay composites with respect to thermal maturity in type II organic-rich source rocks. Geochimica et Cosmochimica Acta, 2016, 195: 68-83.

Braun, U., Schartel, B., Fichera, M. A. Flame retardancy mechanisms of aluminum phosphinate in combination with melamine polyphosphate and zinc borate in glass-fiber reinforced polyamide 6,6. Polymer Degradation and Stability, 2007, 92(8): 1528-1545.

Campbell, J. H. Pyrolysis of sub-bituminous coal in relation to in-situ coal gasification. Fuel, 1978, 57(4): 217-224.

Choi, E. J., Lim, Y. H., Jeong, Y., et al. Effects of parameters in the preparation of Mo/MWW-type catalysts on the dehydroaromatization of shale gas. Catalysis Today, 2024, 425: 114348.

Chtourou, M., Lahyani, A., Trabelsi, M. Alkaline–modified montmorillonite K10: An efficient catalyst for green condensation reaction of aromatic aldehydes with active methylene compounds. Reaction Kinetics, Mechanisms and Catalysis, 2019, 126(1): 237-247.

Cui, X., Li, M., Chen, X., et al. Effect of addition of K_2CO_3 on the structure of coals with different ranks by FTIR and TG/MS. Journal of Analytical and Applied Pyrolysis, 2023, 172: 106027.

Dai, M., Yu, Z., Fang, S., et al. Behaviors, product characteristics and kinetics of catalytic co-pyrolysis spirulina and oil shale. Energy Conversion Management, 2019, 192: 1-10.

Demirbas, A. Conversion of oil shale to liquid hydrocarbons. Energy Sources, Part A: Recovery, Utilization and Environmental Effects, 2016, 38 (18): 2698-2703.

Faisal, H. M. N., Katti, K. S., Katti, D. R. Modeling the behavior of organic kerogen in the proximity of calcite mineral by molecular dynamics simulations. Energy & Fuels, 2020, 34(3): 2849-2860.

Faure, P., Schlepp, L., Mansuy-Huault, L. Aromatization of organic matter induced by the presence of clays during flash pyrolysis-gas chromatography-mass spectrometry (PyGC–MS): A major analytical artifact. Journal of Analytical and Applied Pyrolysis, 2006, 75(1): 1-10.

Gavrilova, O., Vilu, R., Vallner, L. A life cycle environmental impact assessment of oil shale produced and consumed in Estonia. Resources, Conservation and Recycling, 2010, 55(2): 232-245.

Guo, W., Pan, J., Zhang, X., et al. Experimental and mechanistic study on isothermal oxidative pyrolysis of oil shale. Journal of Analytical and Applied Pyrolysis, 2023, 175: 106215.

Ibarra, J., Palacios, J., Gracia, M., et al. Influence of weathering on the sulfur removal from coal by pyrolysis. Fuel Processing Technology, 1989, 21(1): 63-73.

Jiang, H., Hong, W., Zhang, Y., et al. Behavior, kinetic and product characteristics of the pyrolysis of oil shale catalyzed by cobalt-montmorillonite catalyst. Fuel, 2020, 269: 117468.

Kalu, I. E., Jossou, E., Arthur, E. K., et al. Characterization and mechanical property measurements by instrumented indentation testing of Niger Delta oil shale cuttings. International Journal of Engineering Research in Africa, 2022, 59: 89-100.

Kang, Z., Zhao, Y., Yang, D. Review of oil shale in-situ conversion technology. Applied Energy, 2020a, 269: 115121.

Kang, Z., Zhao, Y., Yang, D., et al. A pilot investigation of pyrolysis from oil and gas extraction from oil shale by in-situ superheated steam injection. Journal Petroleum Science Engineering, 2020b, 186: 106785.

Kattai, V., Lokk, U. Historical review of the kukersite oil shale exploration in Estonia. Oil Shale, 1998, 15: 102-110.

Külaots, I., Goldfarb, J. L., Suuberg, E. M. Characterization of Chinese, American and Estonian oil shale semicokes and their sorptive potential. Fuel, 2010, 89(11): 3300-3306.

Lawal, L. O., Adebayo, A. R., Mahmoud, M., et al. Thermal maturation, mineral catalysis, and gas generation kinetics of carbonate source rock. Journal of Natural Gas Science and Engineering, 2021, 92: 104003.

Lewan, M. D., Dolan, M. P., Curtis, J. B. Effects of smectite on the oil-expulsion efficiency of the Kreyenhagen Shale, San Joaquin Basin, California, based on hydrous-pyrolysis experiments. AAPG Bulletin, 2014, 98(6): 1091-1109.

Li, M., Zeng, F., Zhao, Y., et al. Structural evolution around first coalification jump revealed by TG/MS and FTIR. Energy Sources, Part A: Recovery, Utilization and Environmental Effects, 2017, 39(6): 562-569.

Lorant, F., Largeau, C., Behar, F., et al. Improved kinetic modeling of the early generation of CO_2 from the Boom Clay kerogen. Implications for simulation of CO_2 production upon disposal of high activity nuclear waste. Organic Geochemistry, 2008, 39(9): 1294-1301.

Nei, L., Kruusma, J., Ivask, M., et al. Novel approaches to bioindication of heavy metals in soils contaminated by oil shale wastes. Oil Shale, 2009, 26(3): 424-431.

Novikau, R., Lujaniene, G. Adsorption behaviour of pollutants: Heavy metals, radionuclides, organic pollutants, on clays and their minerals (raw, modified and treated): A review. Journal of Environmental Management, 2022, 309: 114685.

Pan, L., Dai, F., Huang, P., et al. Study of the effect of mineral matters on the thermal decomposition of Jimsar oil shale using TG-MS. Thermochimica Acta, 2016, 627-629: 31-38.

Park, Y. K., Siddiqui, M. Z., Karagöz, S., et al. In-situ catalytic co-pyrolysis of kukersite oil shale with black pine wood over acid zeolites. Journal of Analytical and Applied Pyrolysis, 2021, 155: 105050.

Rahman, H. M., Kennedy, M., Löhr, S., et al. The influence of shale depositional fabric on the kinetics of hydrocarbon generation through control of mineral surface contact area on clay catalysis. Geochimica et Cosmochimica Acta, 2018a, 220: 429-448.

Rahman, M. M., Liu, R., Cai, J. Catalytic fast pyrolysis of biomass over zeolites for high-quality bio-oil-A review. Fuel Processing Technology, 2018b, 180: 32-46.

Ramsay, T. Uncertainty quantification of an explicitly coupled multiphysics simulation of in-situ pyrolysis by radio frequency heating in oil shale. SPE Journal, 2020, 25(3): 1443-1461.

Ramsay, T. S. Multiphysics simulation of phase field interface development and geomechanical deformation in radio frequency heating of oil shale. Finite Elements in Analysis and Design, 2021, 191: 103563.

Raukas, A., Punning, J. M. Environmental problems in the Estonian oil shale industry. Energy & Environmental Science, 2009, 2(7): 723-728.

Razvigorova, M., Budinova, T., Tsyntsarski, B., et al. The composition of acids in bitumen and in products from saponification of kerogen: Investigation of their role as connecting kerogen and mineral matrix. International Journal of Coal Geology, 2008, 76(3): 243-249.

Ritchie, R. G. S., Roche, R. S., Steedman, W. Non-isothermal programmed pyrolysis studies of oil sand bitumens and bitumen fractions. 1. Athabasca asphaltene. Fuel, 1985, 64(3): 391-399.

Shi, K., Chen, J., Pang, X., et al. Average molecular structure model of shale kerogen: Experimental characterization, structural reconstruction, and pyrolysis analysis. Fuel, 2024, 355: 129474.

Soerensen, K. J., Cant, N. W. The role of catalysis by mineral matter during oil shale retorting. Fuel, 1988, 67(10): 1344-1348.

Sun, Q., Li, W., Chen, H., et al. Thermogravimetric-mass spectrometric study of the pyrolysis behavior of Shenmu macerals under hydrogen and argon. Energy Sources, Part A: Recovery, Utilization and Environmental Effects, 2006, 28(14): 1281-1294.

Wang, G., Yang, D., Zhao, Y., et al. Experimental investigation on anisotropic permeability and its relationship with anisotropic thermal cracking of oil shale under high temperature and triaxial stress. Applied Thermal Engineering, 2019, 146: 718-725.

Williams, P. T., Chishti, H. M. Influence of residence time and catalyst regeneration on the pyrolysis-zeolite catalysis of oil shale. Journal of Analytical and Applied Pyrolysis, 2001, 60(2): 187-203.

Zhang, H., Wang, S., Shi, C., et al. Evolution characteristics of products retorted from Gonghe oil shale based on TG-FTIR and Py-GC/MS. Thermochimica Acta, 2022, 716: 179325.